# Cobalt exposure via skin alters lung immune cells and enhances pulmonary responses to cobalt in mice

**Running title:** Skin exposure to cobalt alters lung immune cells

Hung-Chang Tsui[1], Tatjana Decaesteker[2], Anne-Charlotte Jonckheere[3], Greetje Vande Velde[4], Jonathan Cremer[5], Erik Verbeken[6], Peter H.M. Hoet[1], Benoit Nemery[1*], Jeroen A.J. Vanoirbeek[1*]

[1] Centre for Environment and Health, Department of Public Health and Primary Care, KU Leuven, Leuven, Belgium.
[2] Laboratory of Respiratory Diseases and Thoracic Surgery (BREATHE), Department of Chronic Diseases and Metabolism, KU Leuven, Leuven, Belgium.
[3] Allergy and Clinical Immunology Research group, Department of Microbiology and Immunology, KU Leuven, Leuven, Belgium.
[4] Biomedical MRI, Department of Imaging and Pathology, KU Leuven, Leuven, Belgium.
[5] Translational Research in Gastrointestinal Disorders (TARGID), Department of Chronic Diseases and Metabolism, KU Leuven, Leuven, Belgium.
[6] Translational Cell & Tissue Research, Department of Imaging and Pathology, KU Leuven, Leuven, Belgium.

* Last two authors shares equal responsibility

**Corresponding author:**
Benoit Nemery, PhD
KU Leuven
Department of Public Health and Primary Care
Centre for Environment and Health
Herestraat 49 mailbox 706
3000 Leuven, Belgium
Telephone: +32 16 33 08 01
E-mail: ben.nemery@kuleuven.be

34 Jeroen Vanoirbeek, PhD
35 KU Leuven
36 Department of Public Health and Primary Care
37 Centre for Environment and Health
38 Herestraat 49 mailbox 706
39 3000 Leuven, Belgium
40 Telephone: +32 16 33 01 96
41 E-mail: jeroen.vanoirbeek@kuleuven.be
42

## Statement of contribution

**Hung-Chang Tsui** has conceptualized the design of the study, carried out the data acquisition, analysis and interpretation, drafted the initial manuscript, and approved the final manuscript as submitted.

**Tatjana Decaesteker** has made substantial contributions to data acquisition and analysis, and approved the final manuscript as submitted.

**Anne-Charlotte Jonckheere** has made substantial contributions to data acquisition and analysis regarding flow cytometry, and approved the final manuscript as submitted.

**Greetje Vande Velde** has made substantial contributions to data acquisition, analysis and interpretation regarding computed tomography, has been involved in revising the manuscript critically for important intellectual content, and approved the final manuscript as submitted.

**Jonathan Cremer** has made substantial contributions to data acquisition, analysis and interpretation regarding flow cytometry, and approved the final manuscript as submitted.

**Erik Verbeken** has made substantial contributions to data acquisition, analysis and interpretation regarding histology, and approved the final manuscript as submitted.

**Peter H.M. Hoet** has made substantial contributions to data interpretation, has been involved in revising the manuscript critically for important intellectual content, and approved the final manuscript as submitted.

**Benoit Nemery** has made substantial contributions to study conceptualization and data interpretation, has been involved in revising the manuscript critically for important intellectual content, and approved the final manuscript as submitted.

**Jeroen A.J. Vanoirbeek** has made substantial contributions to study conceptualization, data acquisition, analysis and interpretation, has been involved in revising the manuscript critically for important intellectual content, and approved the final manuscript as submitted.

## Abstract

**Background**: Cobalt has been associated with allergic contact dermatitis and occupational asthma. However, the link between skin exposure and lung responses to cobalt is currently unknown. We investigated the effect of prior dermal sensitization to cobalt on pulmonary physiological and immunological responses after subsequent challenge with cobalt via the airways.

**Methods**: BALB/c mice received epicutaneous applications (25 µl/ear) with 5% $CoCl_2{*}6H_2O$ (Co) or the vehicle (Veh) dimethyl sulfoxide (DMSO) twice; they then received oropharyngeal challenges with 0.05% $CoCl_2{*}6H_2O$ or saline five times, thereby obtaining four groups: Veh/Veh, Co/Veh, Veh/Co and Co/Co. To detect early respiratory responses non-invasively, we performed sequential *in vivo* micro-computed tomography (µCT). One day after the last challenge, we assessed airway hyper-reactivity (AHR) to methacholine, inflammation in bronchoalveolar lavage (BAL), innate lymphoid cells (ILCs) and dendritic cells (DCs) in lung, and serum IgE.

**Result**: Compared with the Veh/Veh-group, the Co/Co-group showed increased µCT-derived lung response, increased AHR to methacholine, mixed neutrophilic and eosinophilic inflammation, elevated monocyte chemoattractant protein-1 (MCP-1) and elevated keratinocyte chemoattractant (KC) in BAL. Flow cytometry in the Co/Co-group demonstrated increased DC, type 1 and type 2 conventional DC (cDC1/cDC2), monocyte-derived DC, increased ILC group 2 and $NCR^-$ILC group 3. The Veh/Co-group showed only increased AHR to methacholine and elevated MCP-1 in BAL, whereas the Co/Veh-group showed increased cDC1 and ILC2 in lung.

**Conclusion**: We conclude that dermal sensitization to cobalt may increase the susceptibility of the lungs to inhaling cobalt. Mechanistically, this enhanced susceptibility involves changes in pulmonary DCs and ILCs.



**Keywords:** cobalt, dendritic cell, innate lymphoid cell, occupational asthma, skin exposure

## Abbreviations

| | |
|---|---|
| AHR | airway hyper-reactivity |
| AUC | area under curve |
| BAL | bronchoalveolar lavage |
| cDC | conventional dendritic cell |
| cDC1 | conventional type 1 DC |
| cDC2 | conventional type 2 DC |
| DC | dendritic cell |
| DMSO | dimethyl sulfoxide |
| ELISA | Enzyme-linked immunosorbent assay |
| FVC | forced vital capacity |
| $FEV_{0.1}$ | forced expiratory volume in 0.1 second |
| IFN-γ | interferon-gamma |
| IL | interleukin |
| ILC | innate lymphoid cell |
| ILC1 | innate lymphoid cell type 1 |
| ILC2 | innate lymphoid cell type 2 |
| ILC3 | innate lymphoid cell type 3 |
| KC | keratinocyte chemoattractant |
| MCP-1 | monocyte chemoattractant protein-1 |
| MIP-2 | macrophage inflammatory protein 2 |
| μCT | micro-computed tomography |
| moDC | monocyte-derived DC |
| NCR | natural cytotoxicity receptor |
| pDC | plasmacytoid dendritic cell |

## 1. Introduction

Cobalt is a transition metal widely used in rechargeable batteries, hard metal industry, jewelry and painting. Five cobalt compounds and cobalt metal itself have been classified as category 1 sensitizers (10). Cobalt chloride has been identified as a potent skin sensitizer (22), based on the mouse local lymph node assay (LLNA). Epidemiological studies have demonstrated a higher risk of asthma in workers exposed to cobalt (20, 28), and several case series of cobalt-induced asthma have also been reported (31, 32).

Although several studies identified cobalt as an asthmagen, the mechanisms are still unclear. In a systematic review of animal studies involving almost 30 chemical sensitizers, we have concluded that respiratory responses – especially airway hyper-reactivity (AHR) – to the administration of a sensitizer via the airways are more pronounced in animals having been previously exposed to the chemical via the skin, compared with controls without prior dermal exposure (33). The evidence for this phenomenon is limited for metals with sensitizing potential.

One of the unresolved questions is whether skin exposure/sensitization to cobalt can lead to asthma-like symptoms when the airways are subsequently exposed to cobalt. In a well-validated mouse model, we have shown this mechanism for several chemicals (37, 39, 7). In animal asthma models, neutrophils and eosinophils in BAL have long been considered as indicators of airway inflammation. Moreover, emerging evidence has revealed the role of innate lymphoid cells (ILCs) (17) and dendritic cells (DCs) (12) in the pathogenesis of asthma.

The hypothesis of this experimental study was that our asthma model consisting of skin sensitization followed by airway challenge, which we had validated for several organic chemicals (33), would also be applicable to a relevant metallic sensitizer, such as cobalt. We also investigated whether a low-dose μCT approach was able to identify early changes in the lungs after the airway challenges in a non-invasive manner. Finally, we assessed for the first time the involvement of innate lymphoid cells (ILC) and dendritic cells (DC) in the immune responses induced in the lungs by prior dermal exposure to a sensitizer.

## 2. Materials and Methods

### 2.1 Animals

Male BALB/cAnNCrl mice (6-8 weeks old) were purchased from Charles Rivers Laboratories (Germany). All mice were housed in a conventional animal house with 14h light/10h dark cycles, in individually ventilated cages (n=3-4 per cage). They received water and pelleted food *ad libitum*. All animal procedures were approved by the KU Leuven Ethical Committee for animal experiments (P135/2017).

### 2.2 Reagents

Cobalt (II) chloride hexahydrate ($CoCl_2{*}6H_2O$) (CAS 7791-13-1), dimethyl sulfoxide (DMSO) (CAS 67-68-5), and acetyl-β-methylcholine (methacholine) were obtained from Sigma-Aldrich (Bornem, Belgium). The concentration of $CoCl_2{*}6H_2O$ is given as percentage (w/v) in dissolving vehicle (1% $CoCl_2{*}6H_2O$=42mM).

### 2.3 Experimental protocols

The choice of concentrations (and vehicle) for skin application and oropharyngeal instillations were based on preliminary dose-finding experiments described in a supplement (Figure S1, https://doi.org/10.6084/m9.figshare.12403838). Two preliminary experiments were conducted. In the first preliminary experiment, 25 μL $CoCl_2{*}6H_2O$ (0.625%, 1.25%, 2.5% and 5%) or DMSO vehicle were applied on both ears of mice (n=4~6 per concentration) on days 1 and 8. On day 15, the auricular lymph nodes were collected for the analysis of lymphocyte subtypes. In the second preliminary experiment, the mice received one oropharyngeal instillation with 50 μL $CoCl_2{*}6H_2O$ (0.0625%, 0.125%, and 0.25%) or saline vehicle (n=3 per concentration) under light isoflurane inhalation. One day later, the bronchoalveolar lavage (BAL) was collected to analyze the pulmonary inflammation. In both preliminary experiments, blood was also collected to analyze the immunoglobulins.

Based on these results (mainly increased total IgE) and literature data (14), we chose a concentration of 5% $CoCl_2{*}6H_2O$ in DMSO to achieve dermal sensitization. We chose a concentration of 0.05% $CoCl_2{*}6H_2O$ in saline for oropharyngeal challenges because this concentration caused only mild airway inflammation (<10% neutrophils in BAL) 24 h after a single administration, thus allowing us to distinguish inflammation caused by an allergic response from that caused by nonspecific irritation.

We did two series of experiments, each following similar treatment protocols (Figure 1) and having 6 to 9 mice per group. Mice were divided into four groups based on whether they received 1) initial skin exposure to $CoCl_2$ (Co) or vehicle (Veh) and/or 2) oropharyngeal instillation of $CoCl_2$ or vehicle. On days 1 and 8, the mice received 25 µL of 5% $CoCl_2{*}6H_2O$ (310 µg $Co^{2+}$) or vehicle (DMSO) on each ear. On days 15, 17, 19, 22 and 24, the mice received an oropharyngeal instillation of 50 µL of 0.05% $CoCl_2{*}6H_2O$ (6 µg $Co^{2+}$) or vehicle (saline). This led to the following four groups: Veh/Veh, Veh/Co, Co/Veh, and Co/Co.

In the first series, we performed sequential µCT, and assessed pulmonary function, immune cell distribution in the auricular lymph nodes, and lung histology. In the second series, we analyzed the innate lymphoid cells (ILCs) and the dendritic cells (DCs) in lung tissue. In both series, we evaluated total IgE, IgG1 and IgG2 in the serum, and cytokines and cell subtypes in BAL.

## 2.4 Lung imaging analysis with micro-computed tomography (µCT)

On day 1 (before the dermal sensitization), day 9 (24h after the second dermal sensitization), day 16 (24h after the first challenge) and day 25 (24h after the last challenge and before the measurement of pulmonary function), mice were anesthetized with 1.5–2% isoflurane in 100% oxygen and placed in supine position in a small-animal µCT scanner (SkyScan 1278, Bruker micro-CT, Kontich, Belgium) to obtain µCT images during free breathing. Each scan takes approximately 3 minutes and is associated with a measured radiation dose of 60-80 mGy, validated to be radiosafe (1).

Scan parameters were 50 kVp X-ray source voltage and 346 µA current combined with a composite X-ray filter of 1 mm aluminium, 150 ms exposure time per projection, acquiring 3 projections per step with 0.9° increments over a total angle of 220°, and 10 cm field of view covering the whole body producing expiratory-weighted 3D data sets with 50 µm isotropic reconstructed voxel size. Three-dimensional micro-CT data were then weighted and reconstructed by using NRecon software (version 1.6.10.4) with the following parameters: Gaussian smoothing of 1, beam hardening correction of 10%, fine-tuning of post alignment and ring artifact reduction applied *ad hoc* if needed.

The main outcome measures were total lung volume, aerated volume, and non-aerated lung volume and mean densities thereof (36). The aerated lung volume was then gated into alveolar and airway volume. The trachea surface was measured at the level of tracheal carina. Lung regions of interest (ROIs) were manually delineated on each coronal image slice,

198 excluding the heart and main blood vessels. ROIs were then converted to binary datasets in
199 the grayscale index histogram, with (51.42 μm)$^3$ voxel size (CTAn, Skyscan, 1.17.7.2).
200 To calibrate Hounsfield unit (HU), we scanned a phantom consisting of an air-filled
201 1.5 ml tube inside a water-filled 50 ml tube. Based on the stacked histogram of water and air,
202 the mean grayscale index of water (130.42) was set to 0 HU, and the grayscale of air (5.68) to
203 -1000 HU. Voxels with HU < -187.75 were gated as aerated lung area (equivalent to
204 grayscale index 0-107); voxels with HU> -187.75 were gated as non-aerated area (equivalent
205 to grayscale index 108-255). In aerated lung area, voxels with HU between -564.55 and -
206 187.75 (equivalent to grayscale index 60-107) were gated as alveolar area; voxels with HU< -
207 564.55 (equivalent to grayscale index 0-60) were gated as airway area.
208
209 ## 2.5 Pulmonary function
210 Twenty-four hours after the last oropharyngeal instillation, AHR was measured by
211 flexiVent (SCIREQ Inc., Montreal Qb, Canada) (34). The system was equipped with a FX1
212 module as well as with a NPFE extension for mice and it was operated by the flexiWare v7.3
213 software. A small particle size Aeroneb Lab nebulizer (2.5–4 μm; Aerogen, Galway, Ireland)
214 was integrated in the inspiratory arm of the Y-tubing for the generation of the aerosol
215 challenges. The nebulizer activation was synchronized with inspiration and set to a 50% duty
216 cycle for 5 s. Mice were anesthetized by injecting pentobarbital (Dolethal, 70 mg/kg body
217 weight). Parameters were acquired before and after nebulization of methacholine (0, 1.25, 2.5,
218 5, 10, or 20 mg/mL) in saline.
219 Airway resistance (Newtonian resistance, Rn) was measured via Quick Prime-3 (QP3)
220 perturbation. After each methacholine concentration, the QP3 perturbation was performed 5
221 times spread over 2 min. If the coefficient of determination of a QP3 perturbation was lower
222 than 0.90, the measurement was excluded and not used to calculate the average. Forced vital
223 capacity (FVC) and forced expiratory volume in 0.1 s, ($FEV_{0.1}$) were determined using a
224 negative pressure-driven forced expiratory volume (NPFE) perturbation. The concentration of
225 methacholine causing a 20% drop in $FEV_{0.1}$ ($PC_{20}$), from $FEV_{0.1}$ at 0 mg/mL methacholine,
226 was determined from linear interpolation by using an algebraic formula (4).
227
228 ## 2.6 Bronchoalveolar lavage
229 After pulmonary function measurements, blood was taken by retro-orbital sampling
230 and the lungs were lavaged *in situ* three times with 0.7 mL sterile saline. The recovered BAL

was pooled and centrifuged (1000 g, 4 °C, 10 min). The supernatant was stored at -80° until analysis, and the pellets were re-suspended with 1 mL saline for differential cell counts. The number of cells was determined using a Bürker hemocytometer. To evaluate the differential cell counts, 250 mL of the re-suspended cells were spun onto microscope slides (300 g, 4°C, 6 min) (Cytospin 3, Shandon, TechGen Zellik, Belgium), air-dried and stained (Diff-Quik1 method, Medical Diagnostics, Düdingen, Germany). For each sample, 200 cells were counted to determine the proportions of macrophages, eosinophils, neutrophils and lymphocytes.

## 2.7 Cytokines

The concentrations of IFN-γ, IL-4, IL-5, IL-10, IL-13, IL-17A, IL-17F, keratinocyte chemoattractant (KC), monocyte chemoattractant protein-1 (MCP-1) and macrophage inflammatory protein 2 (MIP-2) were measured in undiluted BAL, using the MSD U-plex Assay (Meso Scale Diagnostics, Maryland, USA). Measurements were conducted according to manufacturer's instructions. The detection limits were as follows: 0.16 pg/ml (IFN-γ), 0.56 pg/ml (IL-4), 0.63 pg/ml (IL-5), 3.8 pg/ml (IL-10), 2.7 pg/ml (IL-13), 0.30 pg/ml (IL-17A), 24 pg/ml (IL-17F), 4.8 pg/ml (KC), 1.4 pg/ml (MCP-1), 0.3 pg/ml (MIP-2).

## 2.8 Analysis of dendritic cell and innate lymphoid cells in lung

The lungs were collected and rinsed in the digestion medium (26), minced and incubated for 45 minutes at 37°C. Digestion medium consisted of RPMI 1640 supplemented with 5% FCS, 2 mM L-glutamine, 0.05 mM 2-mercaptoethanol [Gibco, Invitrogen, Paisley, United Kingdom], 100 U/ml penicillin, 100 mg/ml streptomycin [Invitrogen], 1 mg/ml collagenase type 2 [Worthington Biochemical, Lakewood, NY], and 0.02 mg/ml DNase I [grade II from bovine pancreas, Boehringer Ingelheim, Ingelheim, Germany]).

Red blood cells were lysed by adding ammonium chloride buffer, and cell yield determined by Bürker hemocytometer. Finally, cells were re-suspended to $10^7$ cells/mL with phosphate buffered saline (PBS). To analyze DCs and ILCs, two million lung cells were pre-incubated with an anti-CD16/CD32 antibody (Clone 2.4G2, BD Biosciences, Erembodegem, Belgium) in order to minimize nonspecific binding. The live/dead staining was performed with the Zombie Aqua™ Fixable Viability Kit.

For DCs subpopulations, cells were labeled with combinations of anti-mouse fluorochrome-conjugated mAbs against CD45 (clone 30-F11), CD11c (clone N418), MHCII (clone M5/114.15.2), CD11b (clone M1/70), CD103 (clone 2E7), CD64 (clone X54-5/7.1)

and Siglec-H (clone 551) (all from Biolegend, San Diego, California). For ILCs subpopulation, cells were stained with a combinations of anti-mouse fluorochrome-conjugated monoclonal antibodies (monoclonal antibodies), which included CD45 (clone 30-F11), CD127 (clone SB/199), CD90.2 (clone 53-2.1), KLRG-1 (clone 2F1) (above from BD Biosciences, Erembodegem, Belgium), NKp46 (Clone 29A1.4) (Biolegend, Koblenz, Germany), and RORγT (Clone AFKJS-9) (ThermoFisher, Merelbeke, Belgium).

In ILCs analysis, antibodies used for lineage exclusion consisted of CD11b (clone M1/70), CD19 (clone 1D3), CD3e (clone G4.18), CD45RB (clone 16A), CD5 (clone 53-7.3), Gr-1 (clone RB6-8C5), TCRγδ (clone GL3), Ter-119 (clone TER-119), and CD94 (clone 20d5) (from either BD Biosciences, Erembodegem, Belgium; or Biolegend, Koblenz, Germany).

The gating strategy of DCs and ILCs is provided in Table 1. DCs were gated into type 1 conventional DC (cDC1), type 2 conventional DC (cDC2), monocyte-derived DC (moDC), and plasmacytoid DC (pDC). ILCs were gated into type 1 (ILC1), type 2 (ILC2), type 3 with positive/negative natural-cytotoxicity-receptor ($NCR^{+}$ILC3/ $NCR^{-}$ILC3). Data acquisition for DCs and ILCs was performed on a LSR Fortessa flow cytometer running DIVA software (BD Biosciences, Erembodegem, Belgium). FlowJo software (BD Bioscience, Ashland, Oregon) was used for data analysis.

## 2.9 Enzyme-linked immunosorbent assay (ELISA)

Blood was sampled from the retro-orbital plexus, and centrifuged at 14000 g, 4 °C, 10 min. The supernatant serum was stored at -80° until analysis. The OptEIA kits (BD Pharmingen™, Erembodegem, Belgium) were used for measuring IgE, IgG1, and IgG2a.

Plates were firstly coated with purified rat anti-mouse IgE (Cat:51-26551E, BD PharmingenTM), IgG1 (Cat: 553445) and IgG2a (Cat: 553446), respectively, before adding samples. Measured target included total serum IgE (diluted 1/100), serum IgG1 (diluted 1/8000) and IgG2a (diluted 1/1000). The optical density values were assessed after the detection antibodies biotinylated rat anti-mouse IgE (Cat: 51-26552), IgG1(Cat: 553441), and IgG2a (Cat: 553388) were added to bind to the analytes. Streptavidin HRPs (Cat: 51-9002813 for IgE, Cat: 554066 for IgG1/G2a) were used to bind to the detection antibodies. A standard curve was created by using mouse IgE (Cat: 51-26556E), IgG1 (Cat: 557273) and IgG2a (Cat: 553454).

## 2.10 Histology

After lavage, the lungs of mice were immersed in 4% formaldehyde after removal from the body. Lung tissue was sliced and stained with hematoxylin and eosin (H&E). Slides were assessed by an experienced pathologist blinded to treatment condition to score inflammation (i.e., infiltration of macrophages/monocytes or leukocytes), epithelial damage (i.e., disruption of the epithelial barrier in the airways), and alveolar widening (airspace enlargements) on a scale of 0–4 (0 for absent; 1 for minor changes; 2 for moderate changes; 3 for substantial changes; and 4 for severe changes).

## 2.11 Lymph node cell suspension and cell subtype differentiation

To examine the influence of cobalt exposure via skin, bilateral auricular lymph nodes from each mouse were collected and kept on ice in RPMI-1640 with Glutamax (Cat: 61870-010, Invitrogen, Merelbeke, Belgium). Cell suspensions were obtained by pressing the lymph nodes through a cell strainer (100 mm) (BD Bioscience, Erembodegem, Belgium) and rinsing with 10 mL tissue culture medium (RPMI-1640). After centrifugation (1000 g, 10 min), cells were counted by using a Bürker hemocytometer and re-suspended as $10^7$ cells/mL in complete tissue culture medium (RPMI-1640 with 10% heat-inactivated fetal bovine serum, 10 mg/mL streptomycin/penicillin). If the cell numbers were fewer than $10^6$, 100 µL complete tissue culture medium was added for suspension.

After the suspension, 500000 cells (or half of the suspension volume if cell numbers were fewer than $10^6$) were stained with anti-CD3+ (APC), anti-CD4+ (APC-Cy7), anti-CD8+ (PerCP-Cy5.5) and anti-CD25+ (PE), or received a single staining with anti-CD19+ (PE) labeled antibodies (BD Biosciences, Erembodegem, Belgium). Percentages of labeled cells were determined by flow cytometry on a LSR Fortessa flow cytometer with DIVA software (BD Biosciences, Erembodegem, Belgium). Data was analyzed by using FlowJo software (TreeStar, Inc, Ashland, Ore). Lymphocytes were gated into B cell ($CD19^+$), T cell ($CD3^+$), T helper cell ($CD3^+$, $CD4^+$), regulatory T cell ($CD3^+$, $CD4^+$, $CD25^+$), and cytotoxic T cell ($CD3^+$, $CD8^+$).

## 2.12 Data analysis

Data were analyzed by non-parametric Kruskal–Wallis test with independent variables being four groups: Veh/Veh, Co/Veh, Veh/Co and Co/Co. When there was significant effect

from the Kruskal–Wallis test, a multiple comparison post-hoc test was conducted. The associations between two variables were analyzed by nonparametric Spearman correlation test.

To analyze results of sequential measurements (μCT and methacholine test) obtained within the same animals, we used two-way ANOVA with repeated measures to test the interaction between 1) type of treatment and time of μCT assessment, or 2) type of treatment and response to methacholine. A level of $p<0.05$ (two tailed) was considered significant.

## 3. Results

### 3.1 Preliminary test

The preliminary test to determine the optimal concentration for dermal sensitization (Figure S1A, https://doi.org/10.6084/m9.figshare.12403838) showed higher serum IgE in the group receiving 5% $CoCl_2{*}6H_2O$ on the ear 7 days after the second exposure, though not statically significant. The percentage of B-lymphocytes, T-lymphocytes and different subtypes of T cells in auricular lymph nodes did not differ among groups.

In the BAL from the preliminary test of respiratory challenge (Figure S1B, https://doi.org/10.6084/m9.figshare.12403838), we observed significant shifting of neutrophils or eosinophils in groups receiving oropharyngeal instillation with 0.125% and 0.25% $CoCl_2{*}6H_2O$.

### 3.2 Longitudinal μCT

The changes in longitudinal μCT results are provided in Figure 2 (Absolute values are provided in the supplementary Figure S2, https://doi.org/10.6084/m9.figshare.12403880). Compared with the Veh/Veh-group, Co/Co treatment significantly modified the total lung volume growth rate (Figure 2A), which was mainly attributed to increases in aerated lung volume. The Veh/Co-group also exhibited a larger aerated lung volume growth than the Veh/Veh-group (Figure 2B). Compared with the aerated lung volume, the contribution of the non-aerated lung in the total lung volume change was minor (Figure 2C). None of the examined mice showed visual evidence of lung infiltration.

The changes in aerated lung volume were mainly due to increases in alveolar volume for cobalt-instilled groups (Figure 2D). The airways of these groups were enlarged, with the change of airway volume in the Co/Co-group significantly larger than the Veh/Veh-group (Figure 2E).

In accordance to the airway volume change, the trachea surface at the first bifurcation showed a trend of larger increase in both groups receiving Co via the airways (Veh/Co and Co/Co) compared with the Veh/Veh control group (Figure 2F). These two groups also showed a trend of lower lung density in both total lung and aerated lung area (Figure 2G & 2H).

### 3.3 Pulmonary hyper-reactivity and inflammation

When assessed on the basis of $FEV_{0.1}$, the Co/Co-group showed higher responses to methacholine compared with either Veh/Veh or Veh/Co-group (Figure 3A). The Co/Co-group

also showed a lower $PC_{20}$ (Figure 3B). When the response to methacholine was assessed by measuring resistance, only the Co/Co-group, not the Veh/Co-group, clearly showed a higher reactivity than the Veh/Veh. (Figure 3C).

The total number of BAL cells did not differ between the four groups, but the completely $CoCl_2$ treated mice (Co/Co-group) showed significantly higher proportions of neutrophils (8±7 %, mean±SD) compared with Veh/Veh control (1±1 %), but not compared with the Veh/Co-group (4±5 %) (Figure 3D). The Co/Co-group also showed higher proportions of eosinophils (4±7 %) than either the Veh/Veh (0±0 %) or the Veh/Co-group (0±0 %).

In terms of the cytokines in BAL, the Co/Co-group had higher levels of KC and MCP-1 compared with the Veh/Veh-group (Figure 3E). When compared with the Veh/Co-group, the Co/Co-group showed higher levels of KC and MIP-2. The Veh/Co-group had increased MCP-1 but decreased MIP-2; KC in this group did not differ from the Veh/Veh control. The levels of IFN-γ, IL-4, IL-5, IL-10, IL-13, IL-17A and IL-17F did not differ among groups.

Although some mice from Veh/Co and Co/Co presented with inflammation in bronchovascular areas, the semi-quantitative histological scores did not differ among groups (Figure S3, https://doi.org/10.6084/m9.figshare.12403889).

As seen in representative scatterplots (Figure 4A) and in Table 2, when considering all individual data, cellular markers of inflammation in BAL (percentages of neutrophils and eosinophils) correlated with lung imaging features (airway volume change assessed by μCT), KC and MCP-1 in BAL, and also with physiological parameters (airway resistance and $FEV_{0.1}$ response to methacholine).

### 3.4 DC and ILC subtypes in lung

In whole lung tissue homogenates, we assessed subsets of DCs and ILCs. The Co/Co-group showed an increased amount of DC compared with the Veh/Veh-group (Figure 5A). In the analysis of DC subtypes, the Co/Co-group showed significantly increased cDC1, cDC2 and moDC compared with Veh/Veh control (Figure 5B), whereas the Co/Veh-group showed increased cDC1. Plasmacytoid DC (pDC) showed a tendency to decrease in the Co/Co and the Co/Veh-groups, but without reaching statistical significance.

The ratio of ILCs of the $CD45^+$ live cells was significantly higher in both the Co/Co and the Co/Veh-groups, compared with the Veh/Veh control (Figure 5C). This was mainly due to an increase of the ILC2 subset in these two groups (Figure 5D). Furthermore, the

Co/Co-group had higher NCR$^-$ILC3 compared with the Veh/Veh control group, and higher ILC1 compared with the Veh/Co-group.

### 3.5 Immunological indicators from auricular lymph nodes and serum

The analysis of lymphocyte subtypes from auricular lymph nodes did not show differences in the numbers of B cells, T cells, or subtypes of T cells. The cytokine levels in the supernatants from lymph nodes did not change significantly in the Co/Co-group. Total serum IgE, IgG1 and IgG2 did not differ between groups.

Although no significant differences were observed in immune responses in auricular lymph nodes and serum, the skin-lung association was apparent from the association analysis. As shown in Table 3 and Figure 4 (B, C and D), individual levels of serum IgE and helper T cells ($CD3^+CD4^+$) in auricular lymph nodes were positively associated with cDC1 and ILC2, and negatively associated with pDC in the lung. On the other hand, regulatory T cells ($CD3^+CD4^+CD25^+$), cytotoxic T cells and B cells in auricular lymph nodes were associated with pDC and ILC1 in the lung.

## 4. Discussion

Our study shows that dermal contact with $CoCl_2$ followed by repeated airway exposure to $CoCl_2$ leads to several hallmarks of asthma, such as airway hyper-reactivity (AHR) and lung inflammation, with characteristics of the type 2 adaptive immune response, in combination with increased cytokines linked to the innate immune system. Moreover, for the first time we show that in an asthma model, early changes in the lungs can be identified by μCT imaging in free-breathing mice.

While the link between skin sensitization and lung susceptibility has been demonstrated for several chemicals (37, 39, 7), this has never been investigated for metals with sensitizing properties. Cobalt-induced asthma has been frequently reported in occupations involving inhalation of cobalt-containing materials, such as hard metal (a composite consisting mainly of tungsten carbide with cobalt) (16, 40, 41). Previous studies of the respiratory toxicity of cobalt have focused on histological or immunological changes (2, 19, 29). However, to our knowledge, no study has investigated the possible role of skin sensitization in the subsequent development of cobalt asthma.

In this study, we included an imaging modality for the first time to investigate whether alterations can be identified in a mouse model of asthma. The advantage of μCT is to provide high-resolution information in living animals repeatedly at relatively low cost, without causing harm to the animal. In mouse models of lung emphysema (elastase) and fibrosis (bleomycin) early alterations can be detected by μCT (5, 36). Moreover, a low-dose scanning protocol was recently developed, allowing radio-safe repeated follow-up of disease progression (35). Our data showed larger total and aerated lung volumes when mice received $CoCl_2$ respiratory challenge after skin exposure with cobalt. We interpret these changes as reflecting early onset lung alterations associated with inflammation.

Increased airway volume and decreased lung density were observed in both groups receiving $CoCl_2$ via the airways. This image pattern, also named paradoxical airway dilation, has been described in several animal models undergoing bronchoconstriction interventions (9, 34). Since we found a correlation between μCT-derived airway enlargement and BAL airway inflammation (Figure 4A and Table 2), airway dilation could serve as a marker of lung inflammation.

Epidemiological studies show that cobalt may induce or exacerbate AHR in humans (38, 27). In our animal model, the Co/Co-group responded more strongly to a methacholine provocation, with a pronounced decrease in $FEV_{0.1}$, than the other mice. This is in agreement with the obstructive pattern of asthmatic murine models (8, 25, 39). To our knowledge, $FEV_{0.1}$ changes in response to methacholine challenge have not been assessed in an occupational asthma model.

Consistent with the increases in airway volume and AHR, mice of the Co/Co-group exhibited an influx of neutrophils and eosinophils in BAL. In contrast, mice of the Veh/Co-group showed only a minor neutrophilic influx, indicating that the mixed neutrophilic/eosinophilic inflammatory response in the Co/Co-group was due to the initial dermal sensitization. Admittedly, a few mice in the Veh/Co-group responded partly like the Co/Co-group, and this may have been due to the repeated instillations of Co.

In the present study, the total dosage of the oropharyngeal challenge (6 μg $Co^{2+}$ given in five doses) was much lower than that in previous animal models (13 μg $Co^{2+}$ for 10 days) (30), but features of a type 2 allergic inflammation still occurred, presumably due to the initial dermal exposure. The eosinophilic inflammatory response in BAL of dermally $CoCl_2$ treated and $CoCl_2$ challenged group has never been reported in animal models. The eosinophilic inflammation produced only in animals with prior dermal contact, even for a short time, strengthens the conclusion that dermal sensitization increases the airway responsiveness to the corresponding chemical allergen.

Although we observed a mixed neutrophilic/eosinophilic lung inflammation, we found that only cytokines linked to neutrophilic inflammation (KC and MCP-1) were increased in the Co/Co-group. KC (also known as CXCL1 or GROα) is a chemokine critical to neutrophil recruitment. This is the first observation in an animal asthma model that BAL KC is associated with prior skin exposure. While we did not find changes in IL-4, IL-5, or IL-13 in BAL for all groups, which are linked to type 2 eosinophilic inflammation, we found higher MCP-1 (also known as CCL2) in both Veh/Co and Co/Co groups. MCP-1 is a cytokine tightly associated with Th2 reaction, being able to induce mast cell degranulation, thereby enhancing AHR (3). Our observation may imply a more important role of MCP-1 in the Th2 reaction compared with IL-4, IL-5 and IL-13. Unexpectedly, in the Veh/Co-group we found a lower

level of MIP-2 (also known as CXCL2), which is critical to neutrophil attraction and secreted mainly by macrophages (6). A possible explanation of the finding is that the immune reaction shifted away from Th1-macrophage axis, thereby leading to downregulated macrophage and MIP-2 downstream. The interaction between macrophage, cytokines and other signaling cells deserves further research.

Dendritic cells and innate lymphoid cells have been investigated extensively in ovalbumin and house dust mite asthma models (11, 15), but have never been studied in murine asthma models exposed to chemicals or metals. The analysis of DCs in lung revealed elevated cDC1 in both Co/Veh and Co/Co groups, while pulmonary cDC2, moDC and total dendritic cells increased only in the Co/Co-group. cDC1 has been demonstrated to modulate Th17 immune responses (42), though its full role to enhance Th2 reaction remains controversial. cDC2s and moDCs are known to facilitate Th2 and Th17 cell differentiation (23, 24), which is also in accordance with the cytokine pattern from our study. Though some studies have evaluated the shifting of pulmonary DC subtypes after respiratory exposure to sensitizing agents (24, 26), the shifting after solely skin exposure has never been reported.

As dendritic cells, the innate lymphoid cells have not been investigated in a skin/lung model. In this study, pulmonary ILC2 numbers increased in both Co/Veh and Co/Co groups. This finding might explain the eosinophilic inflammation in BAL from the Co/Co-group without an elevation of Th2-related cytokines, and imply an association between skin exposure and ILC2/Th2/eosinophil axis. The role of ILC3 in asthma has rarely been studied in animals compared with ILC2. One ILC3 subtype, $NCR^-$ILC3, is known to produce IL-17 (21). In our study, respiratory $CoCl_2$ challenges irrespective of prior dermal contact showed a trend to increase the level of $NCR^-$ILC3 in $CD45^+$ pulmonary cells, admittedly not at a significant level. Only in the Co/Co-group did $NCR^-$ILC3 increase significantly. As shown in Figure 4B, the neutrophil proportion in BAL was positively associated with $NCR^-$ILC3. Together with the inflammatory patterns in BAL and lung, the results imply that the respiratory exposure to cobalt is associated with ILC3/Th17/neutrophil axis.

In spite of the mixed type 2/type 3 inflammatory reaction in airway, other related cytokines in BAL did not increase altogether. We did not observe increasing IL-4/IL-5/IL-13, which are related to ILC2/Th2/eosinophil reaction. Likewise, IL-17A and IL-17F did not increase despite the elevation of KC and prominent neutrophilic reaction in BAL. Other

cytokines associated with asthma, such as IL-22, IL-25, IL-33 might also serve as potential influential factors (13, 18). In addition, it remains to be verified whether the period between the sensitization and challenge plays a role.

Though the mice in the Co/Co-group showed a marked inflammation, the responses varied considerably between animals and some mice did not show inflammation. We did not observe significant cell proliferation of the auricular lymph nodes with concordant cytokine release, or consistent increases in serum IgE from mice of the Co/Co-group. The absence of these responses contrasts with our previous experience in this skin/lung model with applications of TDI, trimellitic anhydride or ammonium persulfate (37, 39, 7). We hypothesize that these "non-responding" mice had not been successfully sensitized, possibly because the cobalt solution in DMSO did not always persist long enough on the ears (in previous studies we always used a mixture of acetone and olive oil as vehicle, but that mixture did not dissolve $CoCl_2$ well). Although a definite indicator of sensitization (e.g. cobalt-specific IgE) is not available, the possibility that some animals were not sensitized is borne out by the correlation analysis showing that despite the relatively low average changes at group level, T helper cells ($CD3^+CD4^+$) in the auricular lymph nodes and serum IgE were positively associated with cDC1 and ILC2 cells in the lung and other immunological/physiological responses in individual animals (Table 3, Figure 4C-D). The intra-individual consistency between the various responses strengthens our conclusion that dermal sensitization to cobalt enhanced the susceptibility of the airways to subsequent challenges.

In conclusion, prior skin exposure to cobalt modulates immune cells in lung, induces airway hyper-reactivity and a mixed neutrophilic/eosinophilic inflammation upon respiratory challenge with Co, which is accompanied by dendritic cells and innate lymphoid cells of the type 2/type 3. This observation with cobalt strengthens the evidence that asthma caused by low-molecular weight agents is not only related to sensitizers reaching the lungs via airway exposure, but also to chemicals sensitizing the body via skin exposure, which increases the susceptibility of the lungs to inhaling sensitizers.

**Acknowledgements:** the authors have no conflict of interest. The first author (Hung-Chang Tsui) received a "Scholarship to Study Abroad" from the Ministry of Education of Taiwan for

553 2 years (2017/May-2019/May) for his PhD track in KU Leuven. This manuscript is part of his
554 PhD progress

## Reference


1. Berghen N, Dekoster K, Marien E, Dabin J, Hillen A, Wouters J, Deferme J, Vosselman T, Tiest E, Lox M, Vanoirbeek J, De Langhe E, Bogaerts R, Hoylaerts M, Lories R, Vande Velde G. Radiosafe micro-computed tomography for longitudinal evaluation of murine disease models. *Sci Rep* 9: 17598, 2019. doi: 10.1038/s41598-019-53876-x.

2. Camner P, Boman A, Johansson A, Lundborg M, Wahlberg JE. Inhalation of cobalt by sensitised guinea pigs: effects on the lungs. *Br J Ind Med* 50: 753–757, 1993.

3. Campbell EM, Charo IF, Kunkel SL, Strieter RM, Boring L, Gosling J, Lukacs NW. Monocyte chemoattractant protein-1 mediates cockroach allergen-induced bronchial hyperreactivity in normal but not CCR2-/- mice: the role of mast cells. *J Immunol Baltim Md 1950* 163: 2160–2167, 1999.

4. Cockcroft DW, Murdock KY, Mink JT. Determination of histamine PC20. Comparison of linear and logarithmic interpolation. *Chest* 84: 505–506, 1983. doi: 10.1378/chest.84.4.505.

5. De Langhe E, Vande Velde G, Hostens J, Himmelreich U, Nemery B, Luyten FP, Vanoirbeek J, Lories RJ. Quantification of lung fibrosis and emphysema in mice using automated micro-computed tomography. *PloS One* 7: e43123, 2012. doi: 10.1371/journal.pone.0043123.

6. De Plaen IG, Han X-B, Liu X, Hsueh W, Ghosh S, May MJ. Lipopolysaccharide induces CXCL2/macrophage inflammatory protein-2 gene expression in enterocytes via NF-κB activation: independence from endogenous TNF-α and platelet-activating factor. *Immunology* 118: 153–163, 2006. doi: 10.1111/j.1365-2567.2006.02344.x.

7. Devos FC, Boonen B, Alpizar YA, Maes T, Hox V, Seys S, Pollaris L, Liston A, Nemery B, Talavera K, Hoet PHM, Vanoirbeek JAJ. Neuro-immune interactions in chemical-induced airway hyperreactivity. *Eur Respir J* 48: 380–392, 2016. doi: 10.1183/13993003.01778-2015.

8. Devos FC, Maaske A, Robichaud A, Pollaris L, Seys S, Lopez CA, Verbeken E, Tenbusch M, Lories R, Nemery B, Hoet PH, Vanoirbeek JA. Forced expiration measurements in mouse models of obstructive and restrictive lung diseases. *Respir Res* 18, 2017. doi: 10.1186/s12931-017-0610-1.

9. Dubsky S, Zosky GR, Perks K, Samarage CR, Henon Y, Hooper SB, Fouras A. Assessment of airway response distribution and paradoxical airway dilation in mice during methacholine challenge. *J Appl Physiol* 122: 503–510, 2016. doi: 10.1152/japplphysiol.00476.2016.

10. ECHA-European Chemical Agency. Annex XC Restriction Report: cobalt carbonate; cobalt di(acetate); cobalt dichloride; cobalt dinitrate; cobalt sulphate [Online]. 2018. https://echa.europa.eu/registry-of-restriction-intentions/-/dislist/details/0b0236e181d575c8 [29 Jul. 2019].

11. Halim TYF, Krauss RH, Sun AC, Takei F. Lung natural helper cells are a critical source of Th2 cell-type cytokines in protease allergen-induced airway inflammation. *Immunity* 36: 451–463, 2012. doi: 10.1016/j.immuni.2011.12.020.

12. Hammad H, Lambrecht BN. Dendritic cells and epithelial cells: linking innate and adaptive immunity in asthma. *Nat Rev Immunol* 8: 193–204, 2008. doi: 10.1038/nri2275.

13. Hirose K, Ito T, Nakajima H. Roles of IL-22 in allergic airway inflammation in mice and humans. *Int Immunol* 30: 413–418, 2018. doi: 10.1093/intimm/dxy010.

14. Ikarashi Y, Ohno K, Tsuchiya T, Nakamura A. Differences of draining lymph node cell proliferation among mice, rats and guinea pigs following exposure to metal allergens. *Toxicology* 76: 283–292, 1992.

15. Klein Wolterink RGJ, Kleinjan A, van Nimwegen M, Bergen I, de Bruijn M, Levani Y, Hendriks RW. Pulmonary innate lymphoid cells are major producers of IL-5 and IL-13 in murine models of allergic asthma. *Eur J Immunol* 42: 1106–1116, 2012. doi: 10.1002/eji.201142018.

16. Krakowiak A, Dudek W, Tarkowski M, Swiderska-Kiełbik S, Nieścierenko E, Pałczyński C. Occupational asthma caused by cobalt chloride in a diamond polisher after cessation of occupational exposure: a case report. *Int J Occup Med Environ Health* 18: 151–158, 2005.

17. Lai D-M, Shu Q, Fan J. The origin and role of innate lymphoid cells in the lung. *Mil Med Res* 3: 25, 2016. doi: 10.1186/s40779-016-0093-2.

18. Lambrecht BN, Hammad H. Asthma: the importance of dysregulated barrier immunity. *Eur J Immunol* 43: 3125–3137, 2013. doi: 10.1002/eji.201343730.

19. Lewis CP, Demedts M, Nemery B. Indices of oxidative stress in hamster lung following exposure to cobalt(II) ions: in vivo and in vitro studies. *Am J Respir Cell Mol Biol* 5: 163–169, 1991. doi: 10.1165/ajrcmb/5.2.163.

20. Linna A, Oksa P, Palmroos P, Roto P, Laippala P, Uitti J. Respiratory health of cobalt production workers. *Am J Ind Med* 44: 124–132, 2003. doi: 10.1002/ajim.10258.

21. Mjösberg J, Spits H. Human innate lymphoid cells. *J Allergy Clin Immunol* 138: 1265–1276, 2016. doi: 10.1016/j.jaci.2016.09.009.

22. NICEATM -National Toxicology Program Interagency Center for the Evaluation of Alternative Toxicological Methods. Murine Local Lymph Node Assay (LLNA) Database [Online]. 2010. http://ntp.niehs.nih.gov/pubhealth/evalatm/test-method-evaluations/immunotoxicity/nonanimal/index.html [24 Nov. 2016].

23. Norimoto A, Hirose K, Iwata A, Tamachi T, Yokota M, Takahashi K, Saijo S, Iwakura Y, Nakajima H. Dectin-2 promotes house dust mite-induced T helper type 2 and type 17 cell differentiation and allergic airway inflammation in mice. *Am J Respir Cell Mol Biol* 51: 201–209, 2014. doi: 10.1165/rcmb.2013-0522OC.

24. Plantinga M, Guilliams M, Vanheerswynghels M, Deswarte K, Branco-Madeira F, Toussaint W, Vanhoutte L, Neyt K, Killeen N, Malissen B, Hammad H, Lambrecht BN. Conventional and monocyte-derived CD11b(+) dendritic cells initiate and maintain T helper 2 cell-mediated immunity to house dust mite allergen. *Immunity* 38: 322–335, 2013. doi: 10.1016/j.immuni.2012.10.016.

25. Pollaris L, Devos F, De Vooght V, Seys S, Nemery B, Hoet PHM, Vanoirbeek JAJ. Toluene diisocyanate and methylene diphenyl diisocyanate: asthmatic response and cross-reactivity in a mouse model. *Arch Toxicol* 90: 1709–1717, 2016. doi: 10.1007/s00204-015-1606-6.

26. Pollaris L, Van Den Broucke S, Decaesteker T, Cremer J, Seys S, Devos FC, Provoost S, Maes T, Verbeken E, Vande Velde G, Nemery B, Hoet PHM, Vanoirbeek JAJ. Dermal exposure determines the outcome of repeated airway exposure in a long-term chemical-induced asthma-like mouse model. *Toxicology* 421: 84–92, 2019. doi: 10.1016/j.tox.2019.05.001.

27. Rehfisch P, Anderson M, Berg P, Lampa E, Nordling Y, Svartengren M, Westberg H, Gunnarsson L-G. Lung function and respiratory symptoms in hard metal workers exposed to cobalt. *J Occup Environ Med* 54: 409–413, 2012. doi: 10.1097/JOM.0b013e31824d2d7e.

28. Roto P. Asthma, symptoms of chronic bronchitis and ventilatory capacity among cobalt and zinc production workers. *Scand J Work Environ Health* 6: 1–49, 1980. doi: 10.5271/sjweh.2641.

29. Saini Y, Greenwood KK, Merrill C, Kim KY, Patial S, Parameswaran N, Harkema JR, LaPres JJ. Acute Cobalt-Induced Lung Injury and the Role of Hypoxia-Inducible Factor 1α in Modulating Inflammation. *Toxicol Sci* 116: 673–681, 2010. doi: 10.1093/toxsci/kfq155.

30. Saini Y, Kim KY, Lewandowski R, Bramble LA, Harkema JR, LaPres JJ. Role of hypoxia-inducible factor 1α in modulating cobalt-induced lung inflammation. *Am J Physiol-Lung Cell Mol Physiol* 298: L139–L147, 2009. doi: 10.1152/ajplung.00252.2009.

31. Sauni R, Linna A, Oksa P, Nordman H, Tuppurainen M, Uitti J. Cobalt asthma--a case series from a cobalt plant. *Occup Med Oxf Engl* 60: 301–306, 2010. doi: 10.1093/occmed/kqq023.

32. Shirakawa T, Kusaka Y, Fujimura N, Goto S, Kato M, Heki S, Morimoto K. Occupational Asthma from Cobalt Sensitivity in Workers Exposed to Hard Metal Dust. *Chest* 95: 29–37, 1989. doi: 10.1378/chest.95.1.29.

33. Tsui H-C, Ronsmans S, De Sadeleer LJ, Hoet PHM, Nemery B, Vanoirbeek JAJ. Skin Exposure Contributes to Chemical-Induced Asthma: What is the Evidence? A Systematic Review of Animal Models. *Allergy Asthma Immunol Res* 12: 579–598, 2020. doi: 10.4168/aair.2020.12.4.579.

34. Van Den Broucke S, Pollaris L, Vande Velde G, Verbeken E, Nemery B, Vanoirbeek J, Hoet P. Irritant-induced asthma to hypochlorite in mice due to impairment of the airway barrier. *Arch Toxicol* 92: 1551–1561, 2018. doi: 10.1007/s00204-018-2161-8.

35. Vande Velde G, De Langhe E, Poelmans J, Bruyndonckx P, d'Agostino E, Verbeken E, Bogaerts R, Lories R, Himmelreich U. Longitudinal in vivo microcomputed tomography of mouse lungs: No evidence for radiotoxicity. *Am J Physiol Lung Cell Mol Physiol* 309: L271-279, 2015. doi: 10.1152/ajplung.00098.2015.

676 36. Vande Velde G, Poelmans J, De Langhe E, Hillen A, Vanoirbeek J, Himmelreich U,
677 Lories RJ. Longitudinal micro-CT provides biomarkers of lung disease that can be used
678 to assess the effect of therapy in preclinical mouse models, and reveal compensatory
679 changes in lung volume. *Dis Model Mech* 9: 91–98, 2016. doi: 10.1242/dmm.020321.

680 37. Vanoirbeek JAJ, Tarkowski M, Vanhooren HM, De Vooght V, Nemery B, Hoet PHM.
681 Validation of a mouse model of chemical-induced asthma using trimellitic anhydride, a
682 respiratory sensitizer, and dinitrochlorobenzene, a dermal sensitizer. *J Allergy Clin*
683 *Immunol* 117: 1090–1097, 2006. doi: 10.1016/j.jaci.2006.01.027.

684 38. Verougstraete V, Mallants A, Buchet J-P, Swennen B, Lison D. Lung function changes
685 in workers exposed to cobalt compounds: a 13-year follow-up. *Am J Respir Crit Care*
686 *Med* 170: 162–166, 2004. doi: 10.1164/rccm.200310-1357OC.

687 39. Vooght VD, Cruz M-J, Haenen S, Wijnhoven K, Muñoz X, Hoet PH, Morell F, Nemery
688 B, Vanoirbeek JA. Ammonium persulfate can initiate an asthmatic response in mice.
689 *Thorax* 65: 252–257, 2010. doi: 10.1136/thx.2009.121293.

690 40. Walters GI, Moore VC, Robertson AS, Burge CBSG, Vellore A-D, Burge PS. An
691 outbreak of occupational asthma due to chromium and cobalt. *Occup Med Oxf Engl* 62:
692 533–540, 2012. doi: 10.1093/occmed/kqs111.

693 41. Walters GI, Robertson AS, Moore VC, Burge PS. Cobalt asthma in metalworkers from
694 an automotive engine valve manufacturer. *Occup Med Oxf Engl* 64: 358–364, 2014. doi:
695 10.1093/occmed/kqu043.

696 42. Zelante T, Wong AYW, Ping TJ, Chen J, Sumatoh HR, Viganò E, Hong Bing Y, Lee B,
697 Zolezzi F, Fric J, Newell EW, Mortellaro A, Poidinger M, Puccetti P, Ricciardi-
698 Castagnoli P. CD103(+) Dendritic Cells Control Th17 Cell Function in the Lung. *Cell*
699 *Rep* 12: 1789–1801, 2015. doi: 10.1016/j.celrep.2015.08.030.

700

**Figure 1. Experimental protocol.** Balb/c mice received skin exposure to dimethyl sulfoxide (DMSO) or 5% $CoCl_2*6H_2O$ (25µL per ear) on days 1 and 8. On day 15, 17, 19, 22, 24, mice received oropharyngeal challenge with saline or 0.05% $CoCl_2*6H_2O$. µCT was performed on day 1 (before the skin exposure), day 9, day 16 and day 25 (before the pulmonary function measurement).

**Figure 2. Longitudinal micro-computed tomography (µCT) quantification of lung response.** Mice were scanned with µCT on day 1, 9, 16 and 25. Value changes of each time point compared with day 1 were calculated. **A)** Change of total lung volume. **B)** Change of aerated lung volume (Hounsfield unit, HU < -188). **C)** Change of non-aerated volume (HU > -188). **D)** Change of alveolar volume (-565 < HU < -188). **E)** Change of airway volume (HU < -565). **F)** Change of cross-sectional area at the level of first airway bifurcation. **G)** Change of total lung density**. H)** Change of aerated lung density. Data are shown as mean. **p*<0.05 compared with the Veh/Veh control group, when the interaction between type of treatment and time of µCT assessment was examined with two-way ANOVA with repeated measures. *n*=6-9 per group.

**Figure 3. Lung function measurement and inflammatory response in bronchoalveolar lavage (BAL). A)** Forced expired volume at 0.1sec ($FEV_{0.1}$) in response to increasing concentrations of methacholine (0-20 mg/mL) were measured 24 h after the last time of oropharyngeal instillation. **B)** Concentration of methacholine causing a 20% drop (PC20) in $FEV_{0.1}$. **C)** Airway resistance in response to increasing concentrations of methacholine. **D)** Percentage of neutrophils, eosinophils and macrophages were calculated from the BAL obtained 24 h after the last time of oropharyngeal instillation. **E)** Levels of keratinocyte chemoattractant (KC), monocyte chemoattractant protein-1 (MCP-1) and macrophage inflammatory protein 2 (MIP-2) in BAL were determined by MSD U-Plex Assay.

Data are shown as mean. **p*<0.05, ** *p*<0.01, *** *p*<0.001, **** *p*<0.0001 compared with the Veh/Veh control group; $^{\#}$p<0.05, $^{\#\#}$p<0.01 compared with the Veh/Co-group, when the interaction between type of treatment and response to methacholine was examined via two-way ANOVA with repeated measures (3A & 3C) or when data were analyzed by Kruskal–Wallis test (3B, 3D & 3E). *n*=6-9 per group for 3A-C; *n*=12-17 per group for 3D-E.

**Figure 4. Representative scatter plots between skin and lung endpoints. A)** Correlation between airway volume change (measured by µCT) on day 25 and percentage neutrophils in bronchoalveolar lavage (BAL). **B)** Correlation between $NCR^-ILC3$ cells in lung and percentage neutrophils in BAL. **C)** Correlation between ILC2 in lung and $CD3^+CD4^+$ cells in auricular lymph node (ALN). **D)** Correlation between ILC2 in lung and serum IgE. Each point represents data from a single animal (total n=6-9). Coefficients are calculated by Spearman correlation. Note that data with a skewed distribution are expressed on a logarithmic scale (Ln).

**Figure 5. Dendritic cells (DCs) and innate lymphoid cells (ILCs) in the lung**. **A)** Percentage of DCs ($CD45^+$, low-autofluorescent, $CD11c^+$, $MHCII^+$) in leukocytes. **B)** Percentage of DC subpopulations in live leukocytes are shown as type 1 conventional DC (cDC1, $CD11b^-$, $CD103^+$), type 2 conventional DC (cDC2, $CD11b^+$ ,$CD103^-$), monocyte-derived DC (moDC, $CD11b^+$, $CD103^-$, $CD64^+$), and plasmacytoid DC (pDC, $CD11b^-$ Siglec-$H^+$). **C)** Percentage of ILCs ($CD45^+$, lineage negative, $CD90.2^+$, $CD127^+$) in leukocytes. **D)** Per mille of ILC subpopulations in live leukocytes are shown as ILC1 ($KLRG1^-$, $NKp46^+$, ROR $\gamma T^-$), ILC2 ($KLRG1^+$), $NCR^+ILC3$ ($KLRG1^-$, $NKp46^+$, ROR $\gamma T^+$) and $NCR^-ILC3$ ($KLRG1^-$, $NKp46^-$, ROR $\gamma T^+$).

Data are shown as mean. **p*<0.05, ** *p*<0.01, *** *p*<0.001, **** *p*<0.0001 compared with the Veh/Veh control group; $^{\#}$*p*<0.05 compared with the Veh/Co-group as analyzed by Kruskal–Wallis test. *n*=6-8 per group.

**Table 1** Gating strategy in the identification of DC and ILC from lung homogenate

| Abbreviation | Cell type | Gating strategy |
|---|---|---|
| DC | Dendritic cell | $CD45^+$, low-autofluorescent, $CD11c^+$ , $MHCII^+$ |
| cDC1 | Type 1 conventional DC | $CD11b^-$, $CD103^+$ |
| cDC2 | Type 2 conventional DC | $CD11b^+$, $CD103^-$ |
| moDC | Monocyte-derived DC | $CD11b^+$, $CD103^-$, $CD64^+$ |
| pDC | Plasmacytoid DC | $CD11b^-$, Siglec-$H^+$ |
| ILC | Innate lymphoid cell | $CD45^+$, lineage negative, $CD90.2^+$, and $CD127^+$ |
| ILC1 | Type 1 innate lymphoid cells | $KLRG1^-$, $NKp46^+$, ROR $\gamma T^-$ |
| ILC2 | Type 2 innate lymphoid cells | $KLRG1^+$ |
| $NCR^+$ILC3 | Type 3 innate lymphoid cells, natural-cytotoxicity-receptor-positive | $KLRG1^-$, $NKp46^+$, ROR $\gamma T^+$ |
| $NCR^-$ILC3 | Type 3 innate lymphoid cells, natural-cytotoxicity-receptor-negative | $KLRG1^-$, $NKp46^-$, ROR $\gamma T^+$ |

**TABLE 2**. Nonparametric Spearman correlation between BAL cells and other variables

| | BAL % neutrophils | BAL % eosinophils | BAL % macrophages |
|---|---|---|---|
| µCT | | | |
| Δ Total lung volume (on day 25) | 0.29 | 0.01 | -0.28 |
| Δ Aerated lung volume (on day 25) | 0.32 | -0.04 | -0.28 |
| Δ Airway volume (on day 25) | 0.55** | 0.52** | -0.66**** |
| Pulmonary function | | | |
| Δ $FEV_{0.1}$ (methacholine 20mg/mL) | -0.14 | -0.39* | 0.32 |
| Δ Rn (methacholine 20mg/mL) | 0.33 | 0.40* | -0.45* |
| BAL cytokines | | | |
| KC | 0.37** | 0.43*** | -0.42*** |
| MCP-1 | 0.63**** | 0.50**** | -0.62**** |
| MIP-2 | 0.15 | 0.08 | -0.18 |

*$p$<0.05 (two-tailed), ** $p$<0.01, *** $p$<0.001, **** $p$<0.0001 analyzed by Spearman correlations of selected individual responses including all animals (n= 6-9)

**TABLE 3**. Nonparametric Spearman correlation between auricular lymph node (LN) cells and lung dendritic cells (DCs)/innate lymphoid cells (ILCs)

| | Serum IgE | Auricular LN $CD3^+$ | Auricular LN $CD3^+CD4^+$ | Auricular LN $CD3^+CD4^+CD25^+$ | Auricular LN $CD3^+CD8^+$ | Auricular LN $CD19^+$ |
|---|---|---|---|---|---|---|
| Lung DCs | | | | | | |
| DC % of CD45+ live cells | -0.03 | 0.16 | 0.11 | -0.51** | -0.26 | -0.10 |
| cDC1 % of CD45+ live cells | 0.50** | 0.47** | 0.38* | 0.12 | 0.14 | 0.15 |
| cDC2 % of CD45+ live cells | 0.16 | 0.20 | 0.17 | -0.29 | -0.17 | -0.09 |
| moDC % of CD45+ live cells | 0.15 | 0.23 | 0.20 | -0.37* | -0.27 | -0.12 |
| pDC % of CD45+ live cells | -0.15 | -0.38* | -0.34 | 0.55** | 0.40* | 0.12 |
| Lung ILCs | | | | | | |
| ILC ‰ of CD45+ live cells | 0.33 | 0.47* | 0.48** | -0.12 | -0.06 | 0.10 |
| ILC1 ‰ of CD45+ live cells | 0.06 | -0.19 | 0.00 | 0.36 | 0.45* | 0.37* |
| ILC2 ‰ of CD45+ live cells | 0.43* | 0.47** | 0.46* | -0.06 | -0.04 | 0.15 |
| $NCR^+$ILC3 ‰ of CD45+ live cells | -0.04 | 0.10 | 0.33 | 0.12 | 0.13 | 0.08 |
| $NCR^-$ILC3 ‰ of CD45+ live cells | -0.18 | 0.18 | 0.30 | -0.27 | -0.09 | -0.07 |

*$p$<0.05 (two-tailed), ** $p$<0.01, *** $p$<0.001, **** $p$<0.0001 analyzed by Spearman correlations of selected individual responses including all animals (n= 6-9)

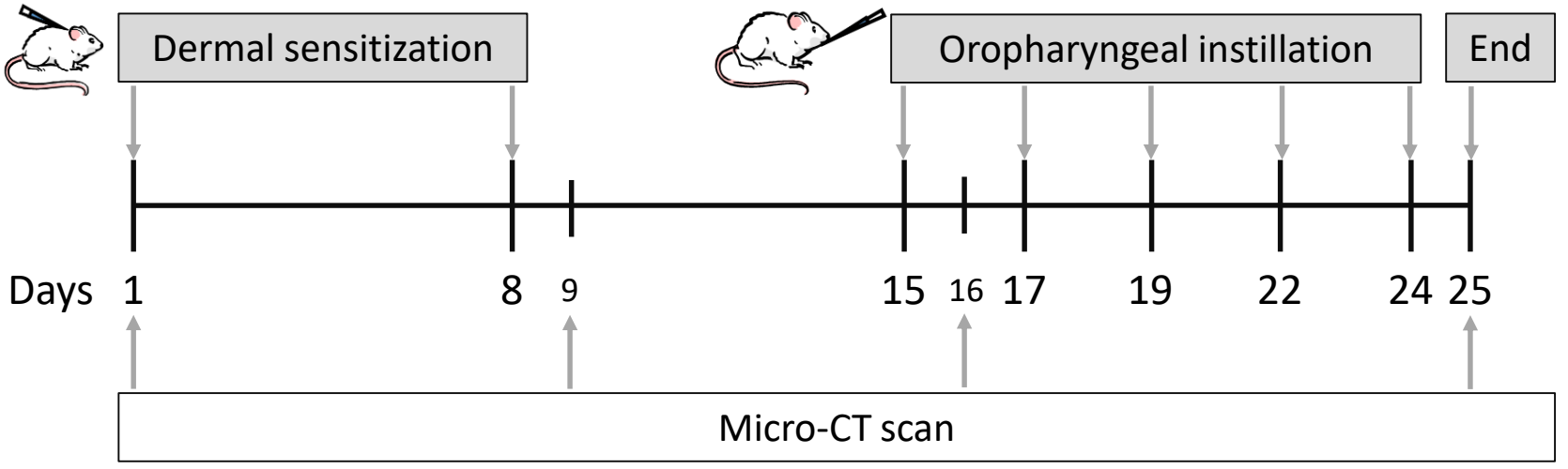


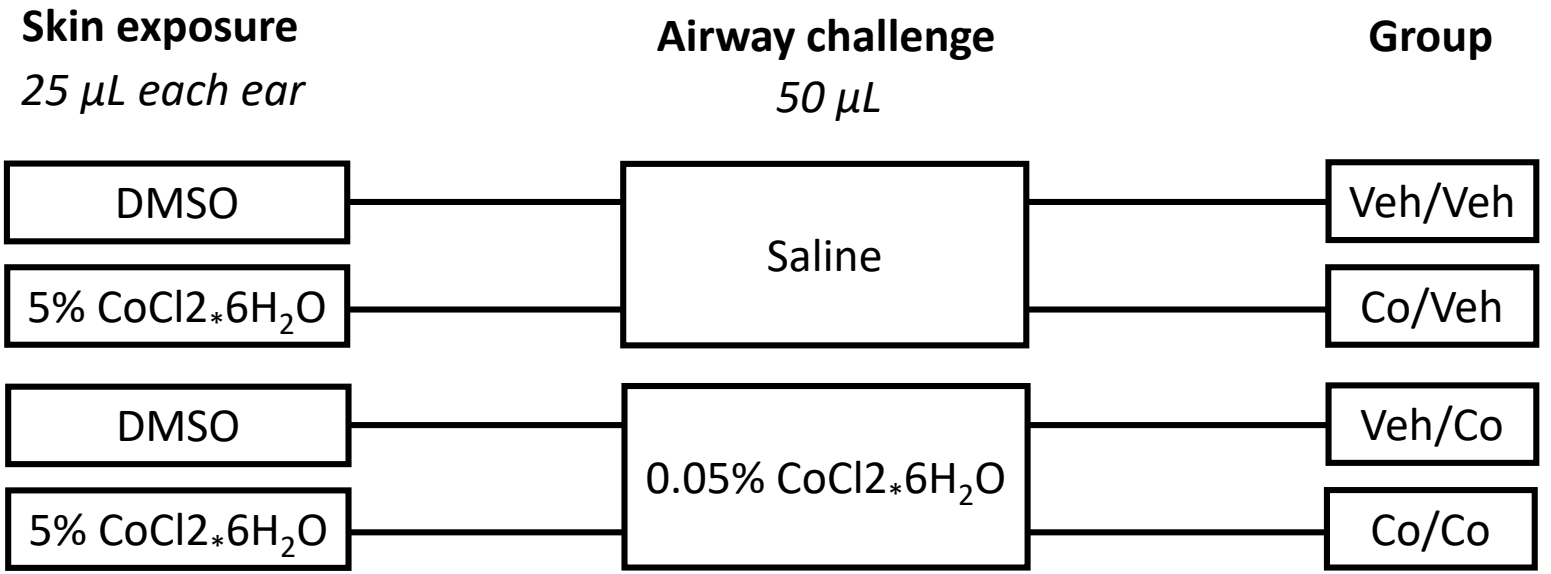


Figure 1

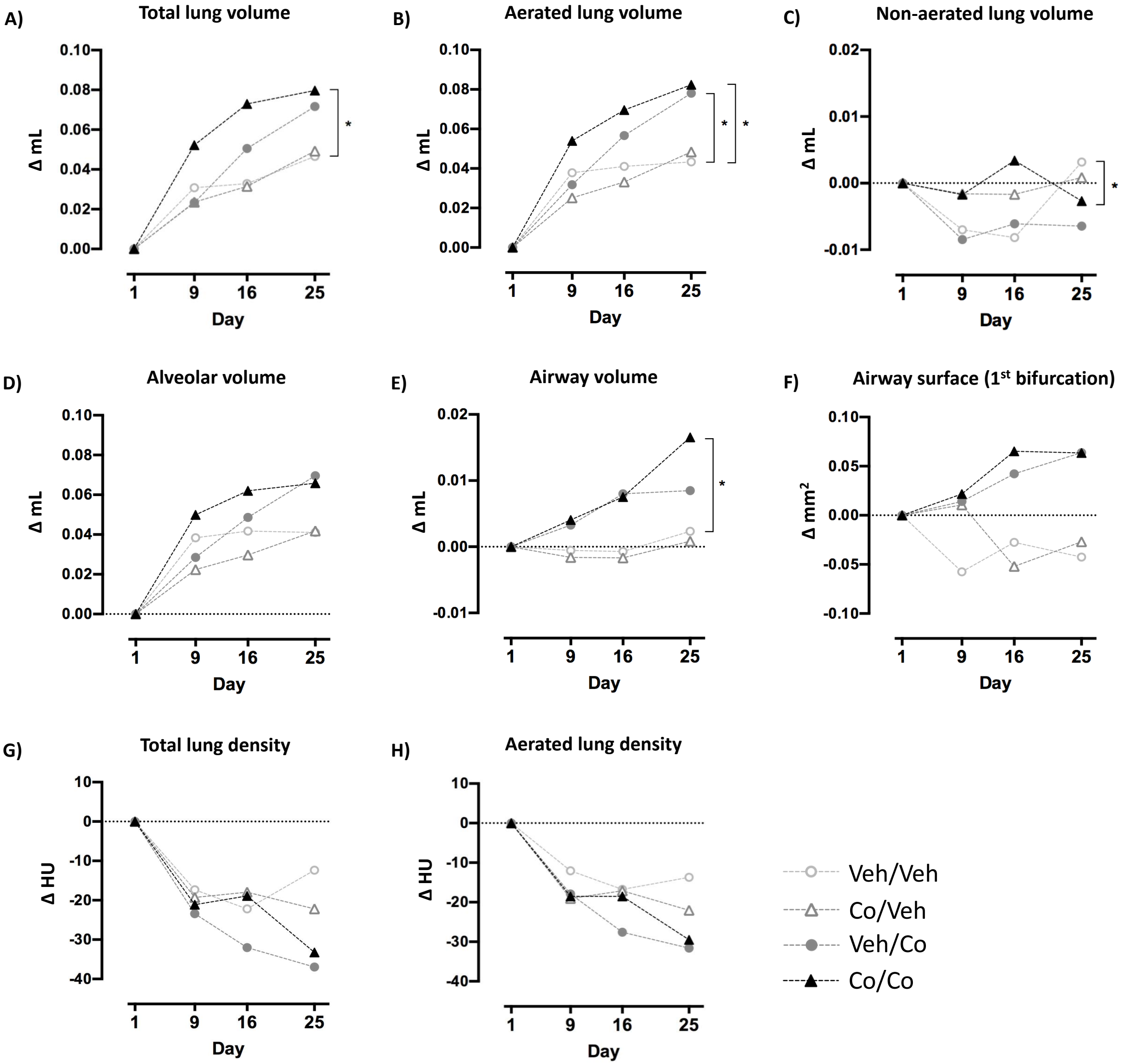


Figure 2

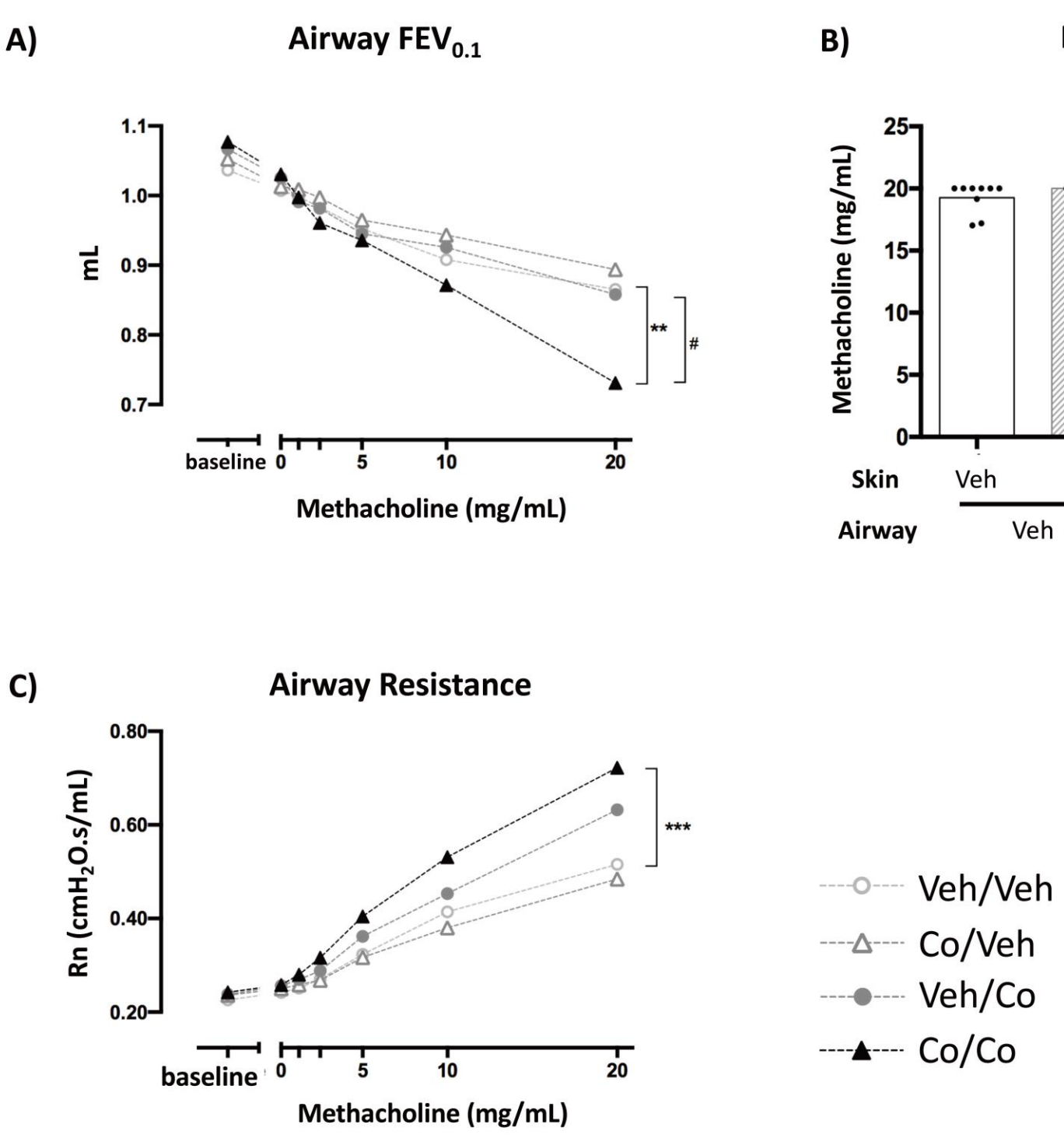


Figure 3

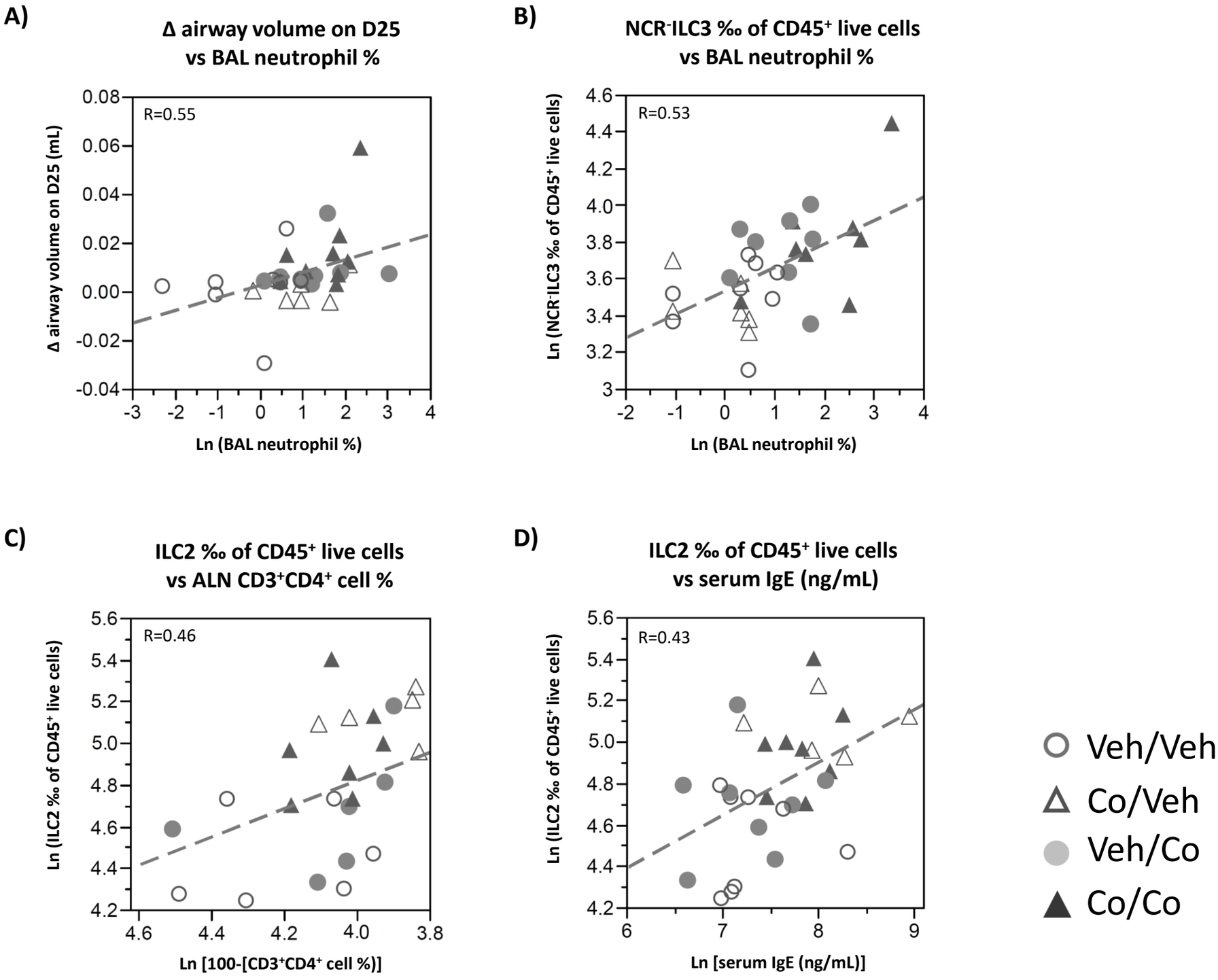


Figure 4

A) DC % of CD45+ live cells

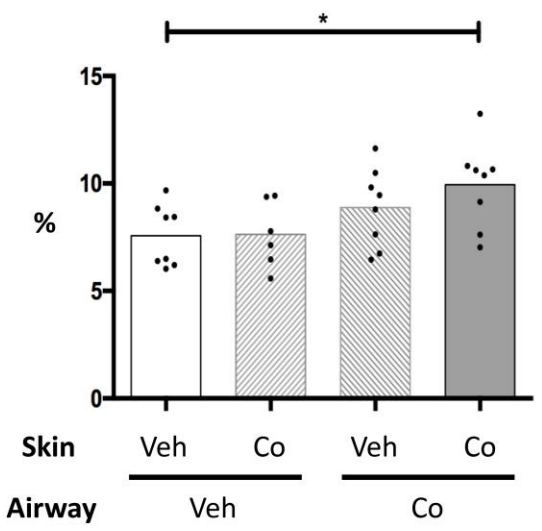


B) cDC1 % of CD45+ live cells

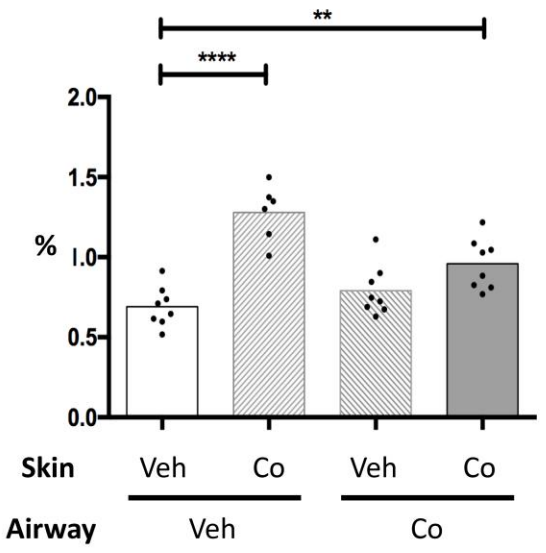


cDC2 % of CD45+ live cells

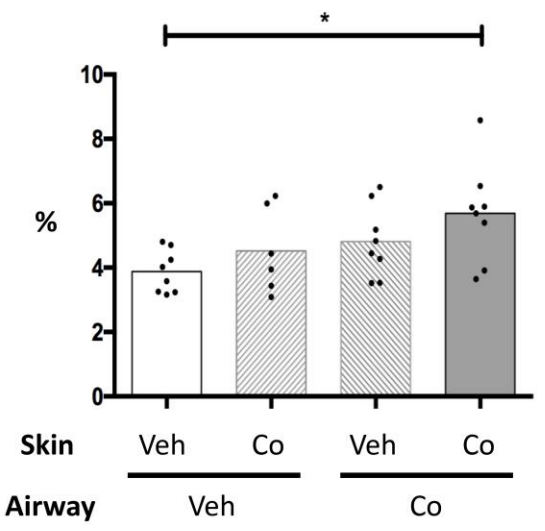


moDC % of CD45+ live cells

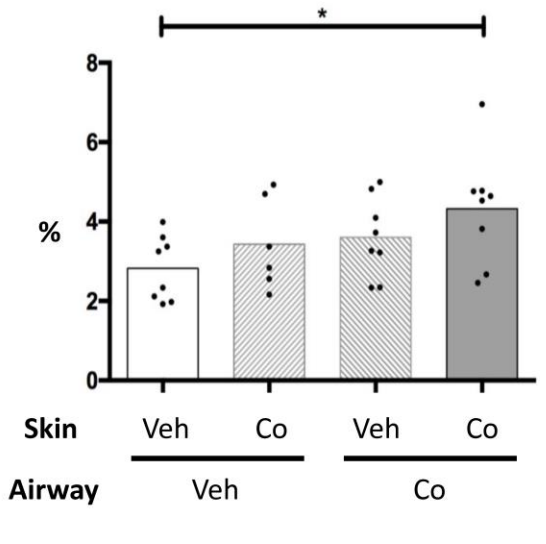


pDC % of CD45+ live cells

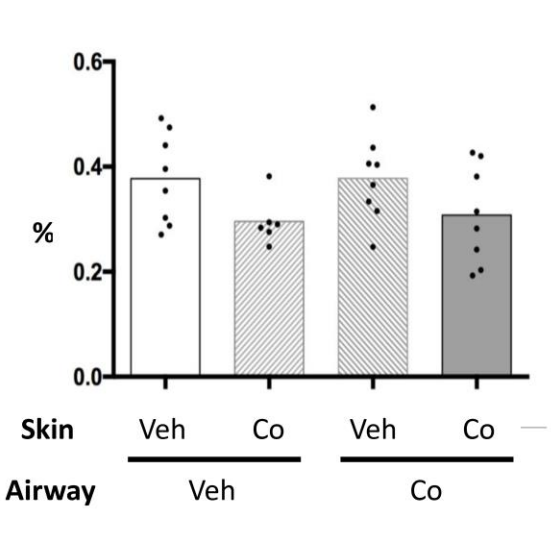


C) ILC ‰ of CD45+ live cells

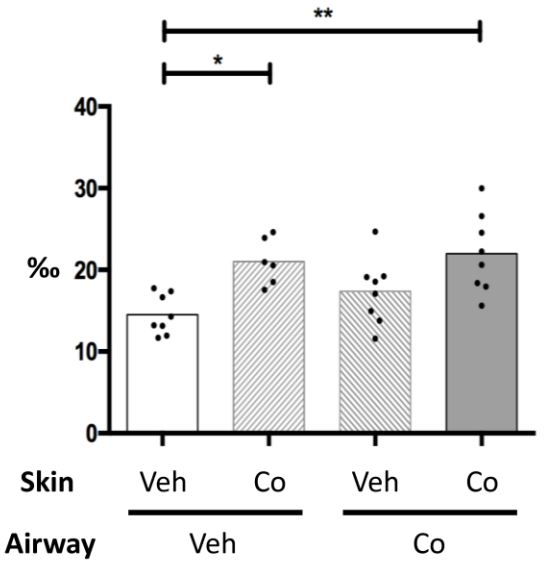


D) ILC1 ‰ of CD45+ live cells

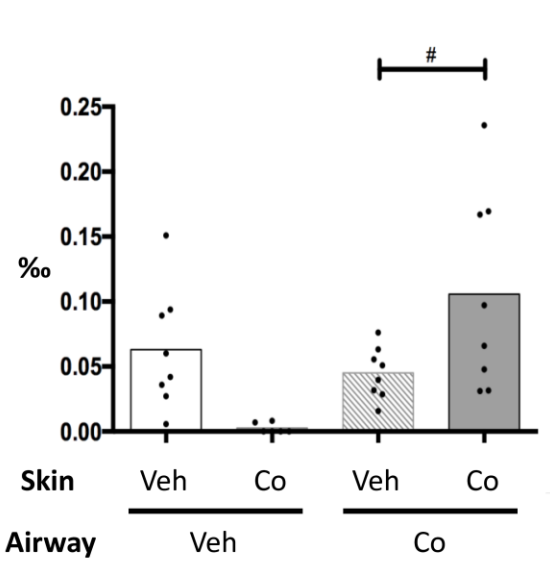


ILC2 ‰ of CD45+ live cells

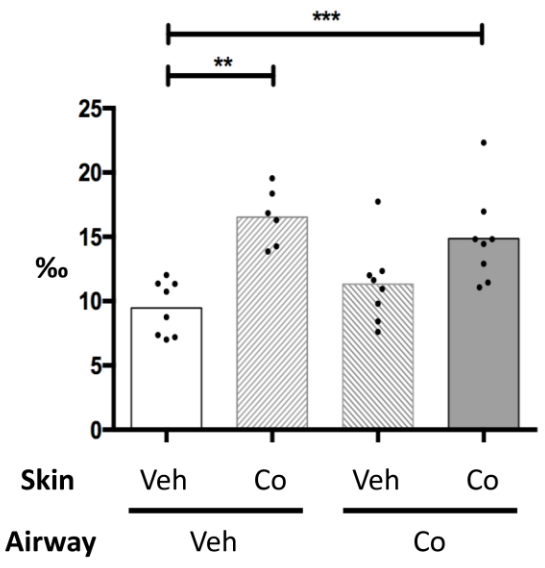


NCR+ILC3 ‰ of CD45+ live cells

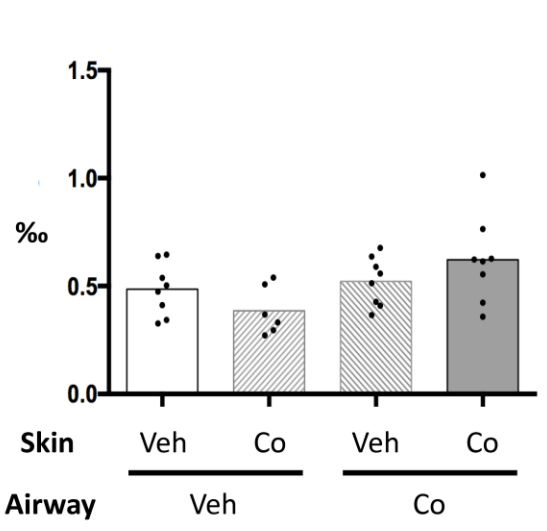


NCR-ILC3 ‰ of CD45+ live cells

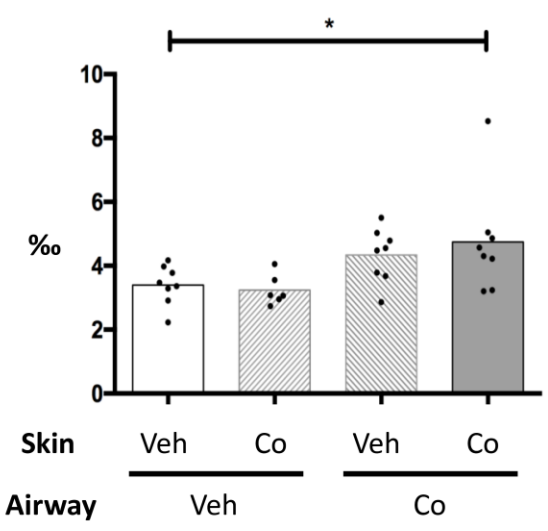


Figure 5